A versatile low-temperature setup for the electrical characterization of single-molecule junctions

Christian A. Martin,[1,2] Roel H. M. Smit,[2] Ruud van Egmond,[2] Herre S. J. van der Zant,[1] and Jan M. van Ruitenbeek[2,a)]
[1]*Kavli Institute of Nanoscience, Delft University of Technology, Lorentzweg 1, 2628 CJ Delft, The Netherlands*
[2]*Kamerlingh Onnes Laboratory, Leiden University, Niels Bohrweg 2, 2333 CA Leiden, The Netherlands*

(Received 17 January 2011; accepted 28 April 2011; published online 27 May 2011)

We present a modular high-vacuum setup for the electrical characterization of single molecules down to liquid helium temperatures. The experimental design is based on microfabricated mechanically controllable break junctions, which offer control over the distance of two electrodes via the bending of a flexible substrate. The actuator part of the setup is divided into two stages. The slow stage is based on a differential screw drive with a large bending range. An amplified piezoceramic actuator forms the fast stage of the setup, which can operate at bending speeds of up to 800 μm/s. In our microfabricated break junctions this is translated into breaking speeds of several 10 nm/s, sufficient for the fast acquisition of large statistical datasets. The bandwidth of the measurement electronics has been optimized to enable fast dI/dV spectroscopy on molecular junctions with resistances up to 100 MΩ. The performance of the setup is demonstrated for a π-conjugated oligo(phenylene-ethynylene)-dithiol molecule. © *2011 American Institute of Physics*. [doi:10.1063/1.3593100]

I. INTRODUCTION

Research in molecular electronics aims at the understanding and, ultimately, the chemical tuning of charge transport across single-molecule junctions.[1] Due to atomic-scale variations in the anchoring of organic molecules to metal electrodes a statistically relevant number of junction configurations has to be probed to unveil electronic structure-property relations. Hence, most two-terminal measurements on molecular junctions are based on the break junction technique in which a metallic contact is repeatedly broken and re-established in the presence of the molecules of interest.[2,3] In this approach, high breaking speeds are essential for acquiring sufficiently large statistical datasets.

Break junction experiments on large organic molecules are usually carried out in modified scanning tunneling microscopes (STMs) or using microfabricated mechanically controllable break junctions (MCBJs). While STMs can break and fuse nanoscale contacts at speeds of up to 100 nm/s, the drift in the piezo elements that control the electrode distance in these setups can be on the order of several Angstroms per minute. This drift reduces the stability of molecular junctions significantly, rendering time-consuming spectroscopic measurements impracticable. Microfabricated MCBJs, in contrast, are exceptionally stable and exhibit drift on the scale of picometers per hour.[4] This low drift is mainly due to the working principle of the mechanical break junction in which the bending of a flexible substrate is translated and attenuated into the stretching of two partially suspended metal electrodes. This mechanical attenuation not only increases the stability, but it also limits the speed of MCBJ experiments. To attain the large bending range required for breaking and fusing the nanoscale contacts, MCBJ setups generally employ slow mechanically driven lead screw actuators, which limits the attainable electrode speed to a few nm/s.[5–7]

Here, we describe the design and performance of a versatile MCBJ measurement system that combines the benefits of high stability and fast actuation. The combination of a screw-based actuator and a mechanically amplified piezo actuator allows for a large dynamic bending range and bending speeds up to 800 μm/s, which are translated to 40 nm/s on the scale of the electrodes. The break junction mechanics are enclosed in a high-vacuum insert that can be immersed in liquid helium for low-temperature experiments. All electrical measurements are carried out using low-noise home-built electronics. During statistical measurements of the conductance of single-molecule junctions a home-built voltage source with a logarithmic current monitor allows for the measurement of currents over more than six orders of magnitude. Spectroscopic lock-in measurements on single-molecule junctions, on the other hand, are facilitated by minimal parasitic capacitances between the wires leading to the junction.

II. DESIGN CONSIDERATIONS

Figure 1(a) presents a schematic of a break junction device in a three-point bending configuration. As the MCBJ device is bent, a thin and partially suspended wire on the substrate surface is stretched and broken at a pre-designed constriction. Subsequently, the electrode distance can be tuned by controlling the bending of the substrate.

The electrode stretching d can be related to the substrate deflection w via the displacement ratio

$$r = \frac{d}{w} = \xi \frac{6 H_S U}{L_S^2}, \tag{1}$$

where H_S, U, and L_S are geometrical parameters of the device and the bending mechanism (see Fig. 1(a)), and the

a)Electronic mail: ruitenbeek@physics.leidenuniv.nl.

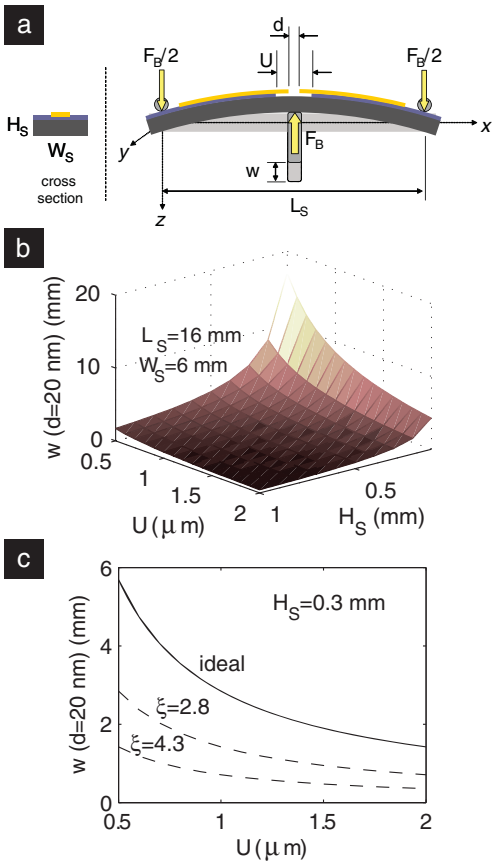

FIG. 1. (Color online) (a) Schematic of a mechanically controllable break junction (MCBJ) with its geometrical parameters. (b) and (c) Mechanical modelling results for different MCBJ designs. The two graphs present the required deflection for an electrode stretching of 20 nm as a function of the substrate thickness H_S and the suspended length U of the electrodes (for phosphor bronze substrates with $L_S = 16$ mm, $W_S = 6$ mm, $E = 120$ GPa). The dashed lines in panel (c) frame the range of values that can be expected from an enhanced displacement ratio according to literature (Ref. 8) (see text).

correction factor $\xi \approx 3 - 4$ accounts for non-uniform deformations in the device structure.[8]

The design of any MCBJ measurement system needs to optimize two figures of merit: the deflection range required to initially break the contact and to tune it between the open and the closed state, and the maximum bending force F_B during this actuation. Both values impose important limitations on the choice of the MCBJ bending actuator (see also the description of the setup below). First and foremost, our design focused on reducing the substrate deflection range that is necessary to modulate the electrode distance over 4 nm, supposedly sufficient for a full breaking and fusing cycle of a molecular junction. In order to fall within the range of a fast piezo actuator, this range should be on the order of a few tens of micrometers. On the other hand, we ensured that the bending force would remain well below 100 N. This value represents a typical operating limit for cryogenic lead-screw actuators.[9] such as the one we use to initially break the contact.

The required deflection for stretching the electrodes by a distance d follows directly from Eq. (1) as

$$w = \frac{L_S^2}{6\xi H_S U} d. \tag{2}$$

The distance L_S of the counter supports in the three-point bending mechanism represents an effective handle for controlling this deflection. To reduce the required bending in our system, the MCBJ substrates were designed to have minimal length while still leaving the junction area accessible for solution deposition processes ($L_S = 16$ mm, $W_S = 6$ mm). This choice allows us to model the influence of the remaining geometrical parameters. As can be seen in Fig. 1(b), the required deflection decreases with increasing substrate thickness H_S. However, the bending force increases quadratically (not shown). To keep the required actuator force small, a substrate thickness of $H_S = 0.3$ mm was chosen. The influence of the remaining design parameter - the suspended length - on the required deflection is presented in Fig. 1(c). The dashed lines in the plot frame the expected range of experimental values that arises from the correction factor ξ.

Based on these calculations, we have chosen the suspended length to be around $U = 2$ μm. The theoretical displacement ratio for this configuration follows immediately from Eq. (1), which yields $r = \xi \cdot 1.4 \times 10^{-5}$. Using a conservative estimate of $\xi = 2.8$ for the experimental enhancement of the displacement ratio,[8] we obtain $r \approx 4 \times 10^{-5}$ and a deflection of $w \approx 0.5$ mm for a junction stretching of $d = 20$ nm. The required dynamic deflection range for the periodic breaking and fusing of the contact over the typical length of a molecule ($d = 4$ nm) is on the order of 100 μm. The expected maximum bending force is around 8 N. These values are all within the target ranges discussed earlier and represent the starting point for the design of our second stage actuator mechanics (see below).

III. DEVICE FABRICATION

The microfabrication of the MCBJ devices for these experiments builds on a process that has been reported earlier.[7] Phosphor bronze wafers (50 mm × 50 mm, thickness 0.3 mm) are polished and cleaned by ultrasonication in acetone and isopropanol. After the application of an adhesion promoter (VM651, HD Microsystems) the wafers are spin-coated with a commercial polyimide precursor solution (PI2610, HD Microsystems). The films are then cured in a vacuum oven to form an insulating and planarizing polyimide layer of 3 μm thickness. For the subsequent electron-beam lithography step, the wafers are spin-coated with a double layer of resist (320 nm methylmethacrylate-methacrylic acid (MMA(17.5)MAA) copolymer, followed by 110 nm polymethylmethacrylate (PMMA) with a molecular weight of 950k; both from Microchem Corporation).

We then define 10 devices on a wafer using a Leica electron-beam pattern generator. Each device contains four break junctions that can be addressed individually. For each break junction, starting from two contact pads, two wide access wires run to the center of the substrate, where they narrow down into a thin bridge that is approximately 100 nm wide and 200 nm long. After exposure, we develop the patterns in a mixture of methyl-isobutyl-ketone and isopropanol (volume ratio 1:3). Electron-beam evaporation is then used to deposit a very thin sticking layer (1 nm of Cr) and the electrode layer (80 nm of Au). After lift-off in hot acetone and

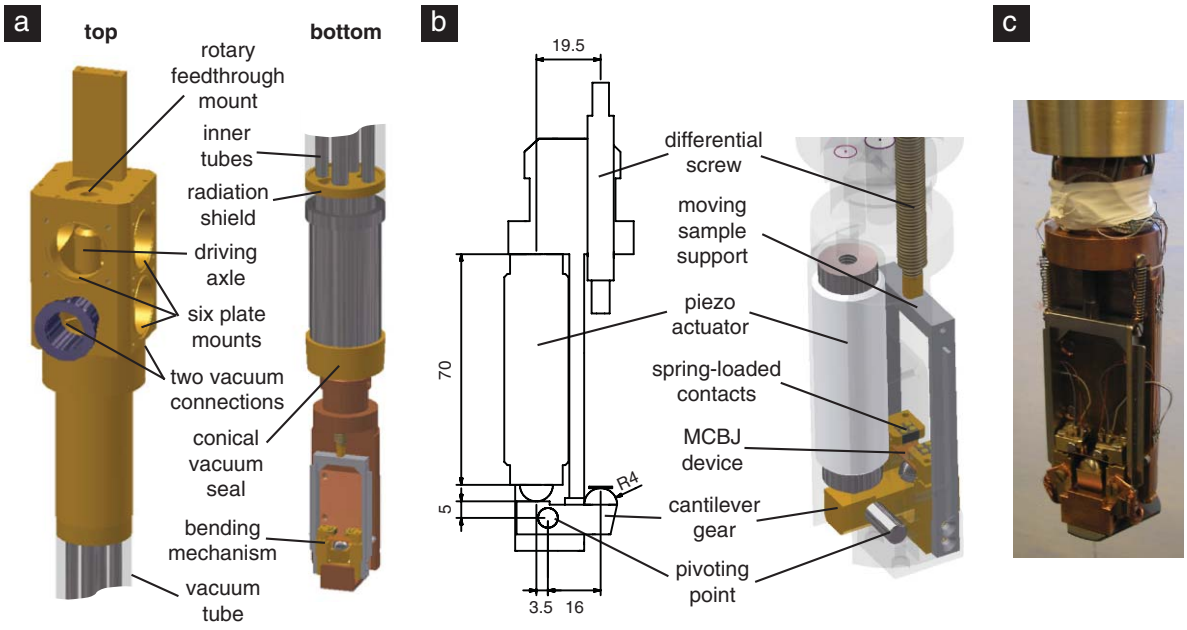

FIG. 2. (Color online) Overview of the vacuum setup used in the MCBJ experiments. (a) Details of the insert. The sample space at the bottom can be closed off with a pot that mates with the conical seal. (b) Details of the MCBJ bending mechanism. The actuator is divided in two stages: a differential screw drive for the coarse and wide-range adjustment of the substrate bending and a fast piezo element with a range of about 280 μm. (c) Photograph of the sample space at the bottom of the assembled insert.

a rinsing step in isopropanol, we protect the fully processed wafers with a 500 nm thick layer of PMMA 350k and remove the individual devices from the wafer using laser-cutting.

The final step of the fabrication process, the undercetching of the electrodes, is carried out on the individual devices immediately before each experiment. We remove the protection layer of the individual devices by immersion in hot acetone, followed by immersion in isopropanol. The devices are then etched in a reactive ion etcher using a mixture of CF_4 and O_2 gas (flow rate ratio around 1:4, pressure 0.2-0.3 mbar, RF power 20-80 W). This results in a nearly isotropic etch profile with a suspended electrode length of about 2 μm.

Although a detailed characterization of the devices lies beyond the scope of this manuscript, we note that the experimental displacement ratio of the bulk-fabricated MBCJs was found to be around 5×10^{-5}. This value is in good agreement with the estimate discussed earlier. A similar device structure with an additional gate electrode in close proximity to the junction has also been developed.[10]

IV. VACUUM INSERT

Figure 2(a) presents an overview of the vacuum insert that can be used at temperatures down to that of liquid helium. For maximum flexibility, the design comprises a modular head to host all vacuum feedthroughs, a central tube section that mates with a pot to form a vacuum sample space at the bottom, and a modular bending mechanism.

The head of the insert is equipped with two vacuum flanges and a rotary feedthrough for the mechanical control of the MCBJ. Six small plate mounts are used for electrical connections to the MCBJ device, the piezo actuator, the thermometers and for future extensions. All modular parts are connected by screws and sealed using rubber O-rings.

The outer shell of the insert is made from a wide (48 mm) stainless steel tube of minimal wall thickness (0.3 mm). It hosts five stainless steel tubes, one of which contains the driving axle of the bending mechanism. The other tubes are used to guide wiring and other connections to the MCBJ device. At distances of about 100 mm, the inner tubes are embedded in brass heat shields that absorb and reflect thermal radiation from the insert head. The bottom of the insert was designed to optimize the thermal anchoring of the MCBJ device. All bulk parts of the actuation mechanism are made from either copper or brass. This increases thermal conduction from the MCBJ device to the conical seal of the vacuum chamber, which is in direct contact with the helium bath in a low-temperature experiment, and effectively cools the device.

The actuator part of the setup has been divided into a coarse and a fine stage. The coarse bending is controlled with a brushless servo motor (Faulhaber 3564K024B) with a precision gearhead (Faulhaber 32/3 S, attenuation 246:1), a digital motor controller (Faulhaber MCBL2006S), and a differential screw drive with a pitch of 150 μm per turn close to the MCBJ device (see Fig. 2(b)). The rotation of the motor is transferred to the screw via a backlash-free insulating elastomer coupling (R+W EKL/5/C), a ferrofluidically sealed rotary feedthrough in the insert head (Rigaku RMS-BS-6) and a rotating axle in the tube section of the insert. At the bottom of the insert, the screw moves the two countersupports of the three-point bending mechanism downwards and effectively deflects the center of the substrate. Two metallic springs,

together with the spring force of the substrate, ensure that the countersupports remain pushed towards the top of the insert and the mechanical reference of the differential screw is well defined. For improved lubrication, the differential screw is partially coated with a cryogenics-compatible tungsten disulfide layer (Dicronite DL-5, Lubrication Sciences International). The minimum step size of the screw drive is about 50 nm, corresponding to about 2.5 pm in electrode distance. During a continuous actuation of the MCBJ, the speed of the servo motor is controlled and the deflection does not suffer from discretization inaccuracies. The screw-based actuator is typically run at speeds from 0.02 to 2 μm/s, which are translated into 1 to 100 pm/s on the scale of the electrodes.

The fine actuator stage is based on a roughly 70 mm long high-voltage piezo stack (Physik Instrumente P-016.40P, nominal expansion 60 μm/1000 V, cryogenics compatible), a high-voltage amplifier (Physik Instrumente E-464) and a cantilever mechanism (see Fig. 2(b)). When a voltage is applied to the piezo stack, it expands and pushes the short end of the cantilever downwards. The cantilever amplifies this displacement by a factor of 4.6 and pushes the center of the MCBJ substrate upwards. Thus, the bending range of the piezo-driven actuator stage is enhanced to 280 μm/1000 V at room temperature, corresponding to a full stretching of about 14 nm on the scale of the electrodes. This range is sufficient for a full breaking and fusing cycle of a MCBJ between the open state and a metallic contact with a conductance of more than 40 G_0. Furthermore, the large-signal response of the piezoceramic actuator is linear for voltage ramps up to 3000 V/s. This value corresponds to an actuation speed of about 800 μm/s or 40 nm/s on the scale of the electrodes for a displacement ratio of 5×10^{-5}. Such high actuation speeds enable a fast cycling of MCBJs and facilitate statistical measurement on single-molecule junctions.

V. CONTROL AND MEASUREMENT ELECTRONICS

The MCBJ setup has been automated using the LabVIEW programming environment (National Instruments). The developed measurement software controls both the motor drive of the screw-based actuator and an ADwin-Gold unit (Jäger Computergesteuerte Messtechnik) that addresses the measurement electronics and the piezo actuator. Besides 16-bit analog-digital (AD) and digital-analog converters the ADwin unit hosts an on-board digital signal processor than enables real-time analysis and control of all signal levels.

The home-built measurement electronics of the MCBJ setup are enclosed by a shielded rack that can host several modules, such as voltage sources, current sources, current-voltage converters, and voltage amplifiers ("IVVI rack," designed by Raymond Schouten, TU Delft). To reduce interference from the outside the electronics are accessed via optically coupled isolation amplifiers and powered by a separate battery, resulting in full galvanic isolation of the high-vacuum insert. The four junctions on the MCBJ device can be addressed via a home-built matrix box that is connected to the insert head. All signal inputs of the matrix box are equipped with grounding switches to prevent voltage spikes and low-pass filtered with capacitors of 100 pF. The eight wires leading from the matrix box to the device are shielded in groups of four and guided into the insert via a 24-pole connector (Fischer 105A093). Connections inside the insert are made via 100 μm-thick phosphor bronze wires to reduce heat conduction to the MCBJ device. At the bottom of the insert, all wires are connected to thermalization striplines and guided on to eight gold-plated spring-loaded contacts.

Along the insert the eight measurement wires are spatially separated from the piezo wiring. Moreover, the piezo is isolated from the insert. The piezo signal is guided via a coaxial cable, a floating high-voltage feedthrough in the insert head (CeramTec SHV 5KV), and a 2 mm thin coaxial cable to the bottom of the insert. Both signal wires are connected to thermalization striplines before the connection to the piezo is made.

The inset in Fig. 4(b) presents a schematic of the measurement circuit for a typical break junction experiment, the acquisition and subsequent statistical analysis of conductance traces during the breaking of the contact. The junction conductance is calculated from the junction current and the bias voltage. For these measurements, a dedicated multipurpose voltage source module has been developed (modified module "S4c," designed by Raymond Schouten, TU Delft). When the module is used as a unipolar voltage source in conductance trace measurements, currents across more than six orders of magnitude can be measured with a temperature drift-compensated logarithmic current monitor. Pointwise calibration with standard resistors ranging from 100 Ω to 1 GΩ ensures the accuracy of the measurement, similar to experiments reported by He *et al.*[11] A plot of the characteristics of the logarithmic current monitor and a schematic of the voltage source/current monitor circuit is presented in Fig. 3.

VI. MEASUREMENT PERFORMANCE

The outstanding mechanical performance of the MCBJ setup is reflected in three characteristics: the mechanical stability of the actuator, its small backlash, and the maximum speed of bending.

To test the actuator speed, we have studied the breaking of a clean gold contact in vacuum and at room temperature for different piezo voltage ramps. These conditions are a test case for the single-molecule measurements: at room temperature the surface mobility of adsorbed molecules is large enough to enable the formation of molecular junctions. Therefore, statistical breaking trace measurements are carried out at 300 K rather than at cryogenic temperatures.

Initially, we broke an as-fabricated electrode pair in a clean MCBJ device by bending the substrate with the screw-based actuator. We then applied a bias voltage of 100 mV over the junction and repeatedly broke and fused the contact by ramping the piezo voltage at different rates. In general, the contacts in our break junction devices can be broken and re-established thousands of times. As the piezo voltage increases, the gold contact is stretched and its cross section is reduced. This leads to a decrease in conductance that can be monitored and plotted as a function of time. Figure 4(a) presents examples of the conductance evolution at different voltage ramps. The step-like pattern at the beginning of all

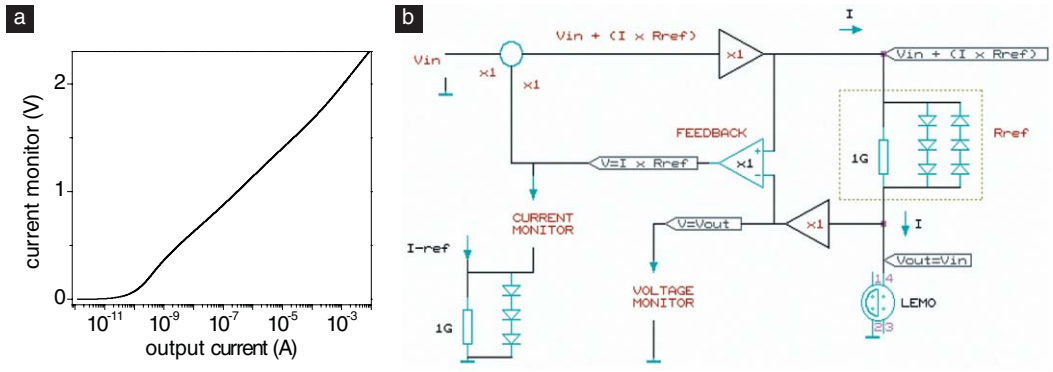

FIG. 3. (Color online) Details of the voltage source module that was designed for wide-range conductance measurements. (a) Calibration curve of the logarithmic current monitor. (b) Simplified schematic of the electronic measurement circuit. The bias voltage is set at the input Vin and supplied via the LEMO connector at the lower right. The reference circuit $Rref$, which contains six diodes of the type FDH300, determines the logarithmic response of the current monitor which can be read out at the left. During unipolar measurements the thermal drift of the current monitor can be compensated by the voltage across the circuit at the lower left, which is typically biased with a current of $I\text{-}ref = 30\ \mu$A.

traces and above the quantum of conductance, $G_0 = 2e^2/h$, can be attributed to stable atomic configurations of the metallic contact. The end of the metallic conductance regime is marked by a recurring plateau at 1 G_0 that can be attributed to the formation of a single-atom contact.[12] As the junction is stretched further, the last gold-gold contact breaks and the junction enters the tunneling regime. This transition is marked by a steep drop in conductance, followed by an exponential conductance decay with increasing electrode distance (see the breaking trace for 30 V/s).

For the acquisition of conductance histograms, the contact was repeatedly cycled between a conductance of 20 G_0 and the open state. Individually sampled data points from the recorded breaking traces then served as the elements in the construction of logarithmic conductance histograms.[5] The entire range of the logarithm of the conductance is split into short intervals, so-called conductance bins. Each time a particular conductance value is recorded the number of counts in the respective bin is increased. In the final histogram, the largest number of counts indicates the most stable junction configuration.

Figure 4(b) presents conductance histograms acquired at piezo ramps from 3 V/s to 3000 V/s, corresponding to bending speeds between 0.8 μm/s and 800 μm/s. On the scale of the electrodes, this is translated into stretching speeds of 0.4 nm/s to 40 nm/s. The dominant peak at 1 G_0 in all histograms indicates the robust formation of single-atom contacts at all these speeds. The histogram background in the sub-G_0 regime is largely featureless, as is typical for a clean device. The larger number of counts below about 10^{-4} G_0 can be attributed to the breaking behaviour of the contacts. Elastic forces in the electrodes lead to a fast jump out of contact after the rupture of the last gold-gold contact and few counts directly below 1 G_0. Following this jump out of contact, the junction conductance decreases exponentially with increasing deflection, as expected for vacuum tunneling; counts from this regime contribute to the higher background at the lower end of the conductance range. For a breaking speed of 3000 V/s, the counts at the lower end of the conductance range are exceptionally high. A close investigation of the breaking traces indicated an unusually slow conductance decay in the tunneling regime, which must be attributed to the settling time of the measurement electronics rather than the behaviour of the contact.

We tested the mechanical stability of our setup by studying a clean MCBJ at cryogenic temperature. We broke the junction and measured the current in the tunneling regime, where the conductance is most sensitive to changes in the electrode distance. The variation in conductance allowed us to derive a distance variation of less than 30 pm in 4 h, similar to

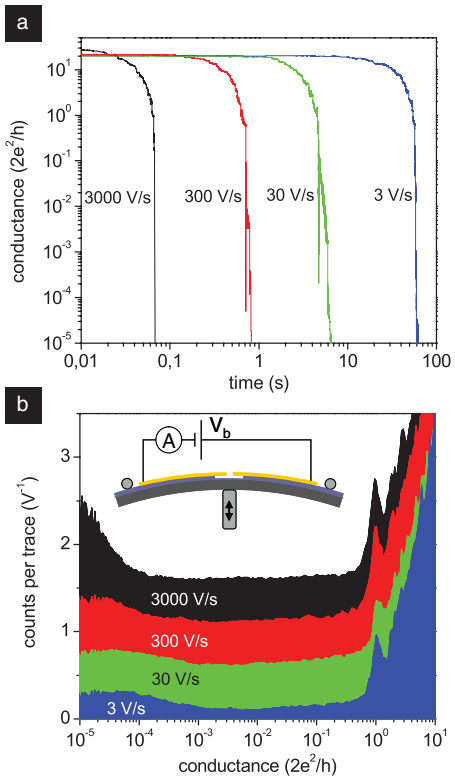

FIG. 4. (Color online) Breaking characteristics of a clean gold MCBJ. (a) Conductance traces during the breaking of the junction at a bias voltage of 0.1 V. The insets indicate the different voltage ramps used for the actuation with the piezo. Two of the curves show some ringing of the logarithmic current monitor. (b) Conductance histograms constructed from 800 consecutive breaking traces. The inset presents a simplified schematic of the measurement circuit used in the acquisition of the data.

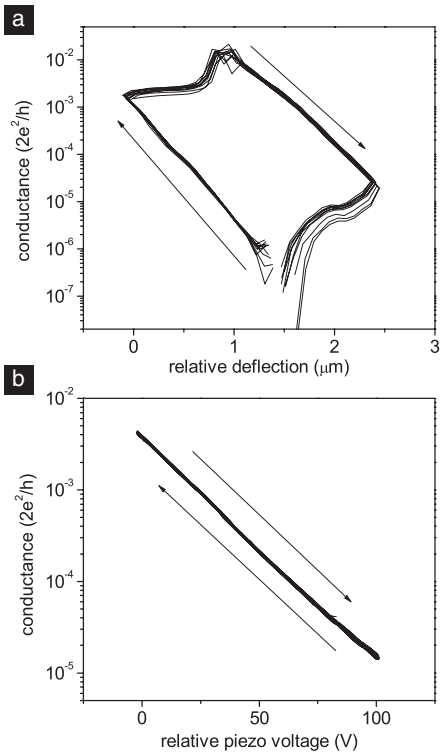

FIG. 5. Backlash characteristics of the screw drive and the piezo actuator at around 4.2 K (0.1 V bias). (a) Tunneling conductance of a clean gold contact upon cycling the screw actuator. (b) Piezo-modulated tunneling characteristics. A triangular voltage signal with a ramping rate of 50 V/s was applied to the piezo.

previous experiments on microfabricated MCBJs. Due to their large displacement ratio, these devices exhibit a very low drift and a good vibration isolation of the suspended electrodes.[4]

Lastly, we obtained information on the mechanical backlash of the actuator from the breaking characteristics of a clean gold sample at cryogenic temperature. Figure 5(a) presents the conductance evolution in the tunneling regime as the bending of the sample is cycled with the screw-based actuator. As the deflection is reduced from about 1.3 μm to 0 μm, the conductance shows the exponential increase typical of vacuum tunneling. Once the direction of the actuation is reversed, the conductance first remains roughly constant and then increases. This non-uniform behaviour upon motion inversion can be attributed to backlash in the servo motor, the gearhead, the differential screw drive, and to the torsional elasticity of the driving axis. Beyond a deflection of 1 μm the exponential tunneling decay of the conductance is recovered. Compared to the increase during the fusing, the curve appears to be shifted by about 1.5 μm, marking the mechanical backlash of the actuator. On the scale of the electrodes, this corresponds to a value of about 100 pm that can be compensated for in actual measurements, leading to a good repeatability of the screw-based actuation.

In contrast to the srew-based actuator stage, the amplified piezo does not exhibit any intrinsic backlash. Its mechanical characteristics are presented in Fig. 5(b). As the piezo voltage is cycled between 0 V and 100 V, the conductance evolution follows a nearly perfect exponential curve, as expected for vacuum tunneling. The slight deviation at the lowest conductances might be due to the logarithmic current monitor, which shows non-exponential characteristics for currents smaller than 100 pA. Clearly, the piezo stage of the actuator offers a higher precision and repeatability. However, at low temperatures its range is limited to a few tens of micrometers.

VII. EXPERIMENTAL PROTOCOL FOR SINGLE-MOLECULE MEASUREMENTS

In the following, we will discuss the experimental protocol for a single-molecule measurement. Immediately after etching the MCBJ devices are dipped into fresh ethanol. This is expected to reduce possible gold oxide on the surface and increase the reproducibility of self-assembly processes.[13,14] The as-fabricated devices are then immersed in a 0.1-1 mM solution of the molecules of interest. The immersion time depends on the anchoring groups of the molecule and may range from a few minutes for dithiols to 24 h for dihioacetates for which we employ no deprotection agents.[15] After the self-assembly process the devices are rinsed in excess amounts of the clean solvent and blown dry. The contact pads are then covered with small droplets of silver paint to prevent scratching by the spring-loaded contacts in the measurement setup. After drying in a desiccator the devices are built into the vacuum insert. To ensure that the electrode surfaces are clean, the first junction is only broken once high vacuum is attained. Our previous experiments on alkanedithiols have shown that the surface mobility of such molecules can be large enough to ensure that they diffuse to the tips of the electrodes, so that electrical contact can be made.[7]

In order to confirm the presence of molecules in the junction area, we first study the device at room temperature. Initially, we run an initialisation procedure using the screw-based actuator stage: After the initial breaking of the gold bridge, we cycle the junction several times between the open state and a conductance of around 50 G_0 until the points at which the junction is broken and fused are reproducible. We then change the method of actuation and measure a conductance histogram by breaking and fusing the junction between the open state and 20 G_0 using the piezo drive. It is important to control the maximum conductance during this histogram measurement, since the probability of forming molecular junctions can be reduced if the contact is fused too far.[7]

Figure 6(a) presents such a conductance histogram for a junction that has been exposed to an oligo(phenyleneethynylene) with acetyl-protected thiol anchoring groups (OPE3) (Ref. 16). The histogram has been constructed from 500 consecutive breaking traces, which took about 90 min to measure. Compared to the characteristics of a clean junction (see Fig. 4), this histogram exhibits a pronounced peak around a conductance of 10^{-4} G_0. It can be attributed to the repeated formation of molecular junctions, which lead to plateaus at this conductance value in the breaking traces. The observation of such a peak marks the presence of molecules in the junction area and is a prerequisite for continuing the experiments at low temperatures.

After the observation of molecular signature in the histogram the junction is cycled further with the screw

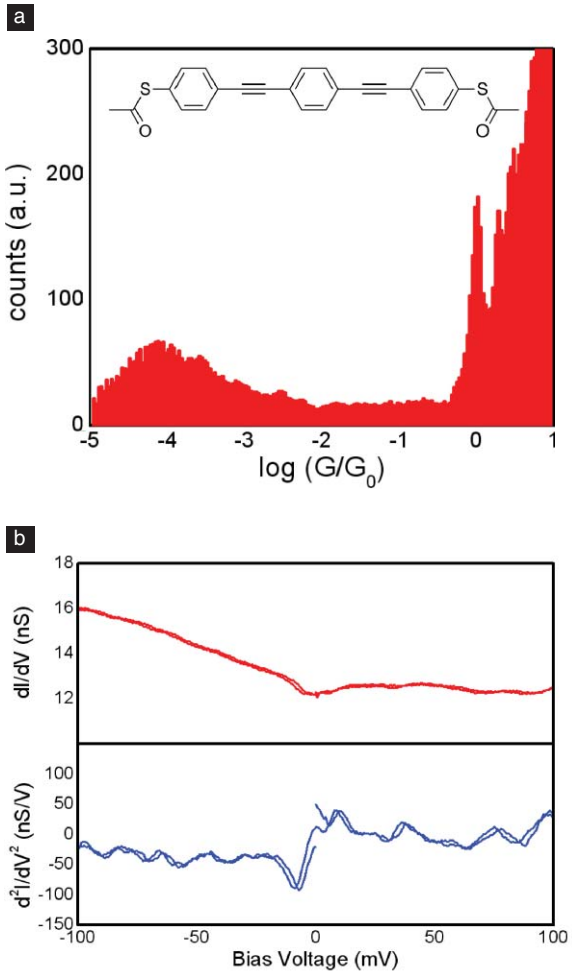

FIG. 6. (Color online) Characteristics of a gold MCBJ after the deposition of OPE3 molecules. (a) Room-temperature conductance histogram at a bias voltage of 0.1 V and a piezo actuation speed of 50 V/s. The inset presents the structure of the molecule. (b) Differential conductance of an OPE3 junction at around 4.2 K. The measurement was carried out using a lock-in amplifier with an excitation of 1 mV at 179 Hz. The second derivative was obtained from a pointwise linear fit of the measured data.

actuator until a breaking trace shows a plateau around the most probable conductance value for the molecular junctions. The junction is then held around that conductance using a feedback loop, and the insert is immersed in liquid helium. Due to differences in the thermal expansion of all mechanical components of the setup it is not always possible to keep the conductance stable at the preset value. However, even if the contact changes, it is usually possible to retrieve the molecular signature at low temperatures.

After cooling down the junction, the bending is cycled again using the screw-based actuator until plateaus in the breaking traces can be observed. Again, it is important not to fuse the junction to more than a few G_0 since the molecules can otherwise be expelled from the junction area. Once molecular signature is observed, the high stability of the setup enables extensive spectroscopic measurements.

An example of a lock-in amplifier measurement of the differential conductance of a molecular junction of OPE3 is presented in Fig. 6(b). The upper panel presents the raw measurement data. Apart from an overall tilt the differential conductance spectrum is quite symmetric around a central dip. The dip is commonly referred to as a zero-bias anomaly and can be observed in both clean and molecular junctions. While the exact origin of this anomaly remains under debate, it may be a sign of environmental Coulomb blockade.[17,18] In nanometer-sized metallic conductors, the interaction of quantum transport channels with the electromagnetic environment can limit the conductance at low temperatures and low electron energies, or bias voltages.

At larger absolute bias voltages, the spectrum displays small, but distinct steps. These steps can be attributed to the excitation of vibrational modes and have been observed for both small gas molecules[2] and large organic molecules.[19] The numerical derivative of the measured data, which is presented in the lower panel of Fig. 6(b), displays a number of peaks at positive bias and dips at negative bias, which allow for a precise location of the vibrational resonances.

VIII. CONCLUSIONS

We have developed a versatile setup for the characterisation of single-molecule junctions down to liquid helium temperatures. In combination with a controlled scheme for trapping molecules at room temperature in vacuum, it enables spectroscopic studies of quantum transport effects such as vibrational modes in large organic molecules. Together with a recently developed sample architecture for gated mechanical break junctions,[10] this setup paves the way for a detailed understanding of the interplay between junction configuration, molecular structure and electric field in the electrical characteristics of single-molecule junctions.

ACKNOWLEDGMENTS

The authors thank Hennie Valkenier and Kees Hummelen for synthesizing and supplying the OPE3 molecules used in this study. They are highly grateful to Raymond Schouten and Bert Crama for expert technical assistance. Moreover, the authors acknowledge Marius Trouwborst, Sense Jan van der Molen, and Cristian Urbina for helpful advice on the setup design. This work is part of the research programme of the Foundation for Fundamental Research on Matter (FOM), which is financially supported by the Netherlands Organisation for Scientific Research (NWO).

[1] S. Lindsay and M. Ratner, Adv. Mater. **19**, 23 (2007).
[2] R. H. M.Smit, Y. Noat, C. Untiedt, N. D. Lang, M. C. van Hemert, and J. M. van Ruitenbeek, Nature (London) **419**, 906 (2002).
[3] B. Xu and N. J. Tao, Science **301**, 1221 (2003).
[4] J. M. van Ruitenbeek, A. Alvarez, I. Piñeyro, C. Grahmann, P. Joyez, M. H. Devoret, D. Esteve, and C. Urbina, Rev. Sci. Instrum. **67**, 108 (1996).
[5] M. T. González, S. Wu, R. Huber, S. J. van der Molen, C. Schönenberger, and M. Calame, Nano Lett. **6**, 2238 (2006).
[6] E. Lörtscher, H. B. Weber, and H. Riel, Phys. Rev. Lett. **98**, 176807 (2007).
[7] C. A. Martin, D. Ding, H. S. J. van der Zant, and J. M. van Ruitenbeek, New J. Phys. **10**, 065008 (2008).
[8] S. A. G. Vrouwe, E. van der Giessen, S. J. van der Molen, D. Dulic, M. L. Trouwborst, and B. J. van Wees, Phys. Rev. B **71**, 035313 (2005)

[9]R.-R. Rohloff, H. Baumeister, M. Ebert, N. Münch, and V. Naranjo, Proc. SPIE **5495**, 636 (2004).
[10]C. A. Martin, J. M. van Ruitenbeek, and H. S. J. van der Zant, Nanotechnology **21**, 265201 (2010).
[11]J. He, O. Sankey, M. Lee, N. Tao, X. Li, and S. Lindsay, Faraday Discuss. **131**, 145 (2005).
[12]N. Agraït, A. L. Yeyati, and J. M. van Ruitenbeek, Phys. Rept. **377**, 81 (2003).
[13]H. Ron, S. Matlis, and I. Rubinstein, Langmuir **14**, 1116 (1998).
[14]H. Ron and I. Rubinstein, Langmuir **10**, 4566 (1994).
[15]H. Valkenier, E. H. Huisman, P. A. van Hal, D. M. de Leeuw, R. C. Chiechi, and J. C. Hummelen, J. Am. Chem. Soc. **133**, 4930 (2011).
[16]N. Stuhr-Hansen, J. K. Srensen, K. Moth-Poulsen, J. Christensen, T. Bjrnholm, and M. Nielsen, Tetrahedron **61**, 12288 (2005).
[17]A. N. Cleland, J. M. Schmidt, and J. Clarke, Phys. Rev. Lett. **64**, 1565 (1990).
[18]A. L. Yeyati, A. Martin-Rodero, D. Esteve, and C. Urbina, Phys. Rev. Lett. **87**, 046802 (2001).
[19]J. Hihath, C. R. Arroyo, G. Rubio-Bollinger, N. Tao, and N. Agraït, Nano Lett. **8**, 1673 (2008).